Control of ciliary transcriptional programs during spermatogenesis by antagonistic transcription factors

Weihua Wang[1,2,5]✉, Junqiao Xing[1,2,5], Xiqi Zhang[1,5], Hongni Liu[1,2], Xingyu Liu[3], Haochen Jiang[1,2], Cheng Xu[1,2], Xue Zhao[1,2], Zhangfeng Hu[1,2,4]✉

[1]Institute of Microalgae Synthetic Biology and Green Manufacturing, School of Life Sciences, Jianghan University, Wuhan, 430056 Hubei, China

[2]Hubei Engineering Research Center for Protection and Utilization of Special Biological Resources in the Hanjiang River Basin, School of Life Sciences, Jianghan University, Wuhan, 430056 Hubei, China

[3]NO.1 Middle School Affiliated to Central China Normal University, Wuhan, 430056 Hubei, China

[4]Hubei Key Laboratory of Environmental and Health Effects of Persistent Toxic Substances, Jianghan University, Wuhan, 430056 Hubei, China

[5]These authors contributed equally: Weihua Wang, Junqiao Xing, Xiqi Zhang

✉ e-mail: wangwh2019@163.com; huzhangfenghzf@163.com

Abstract

Existence of cilia in the last eukaryotic common ancestor (LECA) raises a fundamental question in biology: how the transcriptional regulation of ciliogenesis has evolved? One conceptual answer to this question is by an ancient transcription factor regulating ciliary gene expression in both unicellular and multicellular organisms, but examples of such transcription factors in eukaryotes are lacking. Previously, we showed that an ancient transcription factor XAP5 is required for flagellar assembly in *Chlamydomonas*. Here, we show that XAP5 and XAP5L are two conserved pairs of antagonistic transcription regulators that control ciliary transcriptional programs during spermatogenesis. Male mice lacking either XAP5 or XAP5L display infertility, as a result of meiotic prophase arrest and sperm flagella malformation, respectively. Mechanistically, XAP5 positively regulates the ciliary gene expression by activating the key regulators including FOXJ1 and RFX families during the early stage of spermatogenesis. In contrast, XAP5L negatively regulates the expression of ciliary genes via repressing these ciliary transcription factors during the spermiogenesis stage. Our results provide new insights into the mechanisms by which temporal and spatial transcription regulators are coordinated to control ciliary transcriptional programs during spermatogenesis.

Introduction

Cilia and flagella are evolutionarily conserved hair-like microtubule organelles that project from the surfaces of most eukaryotic cells(Derderian, Canales, & Reiter, 2023; Mitchell, 2017). They play essential roles in sensory reception, signal transduction and cell movement(Goetz & Anderson, 2010; Nachury & Mick, 2019; Singla & Reiter, 2006). The dysfunction of cilia in humans leads to an emerging class of genetic diseases called ciliopathies classified into first-order and second-order ciliopathies(Ishikawa & Marshall, 2011; Lovera & Lüders, 2021; Reiter & Leroux, 2017). First-order ciliopathies are caused by aberrations in ciliary proteins, and second-order ciliopathies occur due to defects in non-ciliary proteins, such as transcription factors, that are required for cilia formation and function(Reiter & Leroux, 2017).

Cilia are complex organelles and are dynamically regulated during development and the cell cycle(Eggenschwiler & Anderson, 2007; Kasahara & Inagaki, 2021; Santos & Reiter, 2008). The transcriptional regulation of ciliary genes must be precisely coordinated during ciliogenesis(Choksi, Lauter, Swoboda, & Roy, 2014; Collins, Ventrella, & Mitchell, 2021; Lewis & Stracker, 2021; Thomas et al., 2010). In metazoans, several transcription factors, including FOXJ1 and RFXs, have been shown to be involved in directing the expression of ciliary genes(Stubbs, Oishi, Izpisua Belmonte, & Kintner, 2008; Swoboda, Adler, & Thomas, 2000; X. Yu, Ng, Habacher, & Roy, 2008). These key ciliary transcription factors show dynamic expression patterns during development and differentiation(Stubbs et al., 2008; Swoboda et al., 2000; X. Yu et al.,

64 2008). However, how these key transcriptional programs are spatially and temporally
65 controlled by cell type-specific transcription factors and signaling pathways in order to
66 activate specific target ciliary genes and generate diverse cilia is largely unknown.

67 Despite transcriptional regulation of ciliary genes is required for ciliogenesis in both
68 unicellular and multicellular organisms, the underlying mechanism mediating ciliary gene
69 expression may be fundamentally different, as the two major transcription factors, FOXJ1
70 and RFXs, are absent from many unicellular organisms(Chu, Baillie, & Chen, 2010; Li et
71 al., 2018; Piasecki, Burghoorn, & Swoboda, 2010; Vij et al., 2012). Cilia and ciliary
72 genes have been highly conserved throughout evolution, suggesting that the regulation of
73 ciliary genes could be programmed by yet undiscovered transcriptional mechanisms,
74 which possibly coevolved with multicellularity. Recently, an ancient transcription factor,
75 XAP5, is found to regulate ciliary gene expression in a unicellular organism,
76 *Chlamydomonas reinhardtii*(Li et al., 2018). XAP5 is highly conserved among different
77 species and is widely expressed across tissues(Martin-Tryon & Harmer, 2008;
78 Mazzarella, Pengue, Yoon, Jones, & Schlessinger, 1997). In vertebrates, *XAP5-like*
79 (*XAP5L*) with an intronless open reading frame originated in Therians via
80 retrotransposition of the ancestral *XAP5*, and it is highly expressed during
81 spermatogenesis(Sedlacek et al., 1999; A. Zhang et al., 2011). However, whether XAP5
82 and XAP5L play essential roles in cilia development in multicellular organisms remains
83 unknown.

84 Here, we show that XAP5/XAP5L are antagonistic transcription factors required for

85 ciliary transcriptional programs during spermatogenesis. XAP5 is widely expressed in
86 different tissues, while XAP5L is exclusively present in the testes. To explore the roles of
87 XAP5/XAP5L in ciliogenesis, we generated a *XAP5L* knockout (KO) mouse line and
88 found that *XAP5L* KO male mice are infertile due to the malformation of sperm flagella.
89 Interestingly, male mice with the loss of XAP5 protein in germ cells also exhibited
90 infertile, due to the arrest of spermatogenesis in the meiotic prophase stage. These data
91 suggest that XAP5/XAP5L play crucial roles in sperm flagellar assembly in a
92 spatiotemporal manner. Mechanistically, XAP5 positively modulates transcriptional
93 rewiring of ciliary genes via activating the key regulators including FOXJ1 and RFXs
94 during the early stage of spermatogenesis. Conversely, XAP5L negatively regulates the
95 transcriptional program controlling ciliogenesis by repressing these ciliary transcription
96 factors during the spermiogenesis stage. Thus, ciliary transcriptional programs are
97 spatially and temporally controlled by XAP5/XAP5L antagonistic transcription factors
98 during spermatogenesis.
99

100 **Results**

101 **XAP5 and XAP5L are indispensable for male fertility**

102 To explore the potential functions of XAP5/XAP5L during ciliogenesis *in vivo*, we
103 performed Western blot analysis to investigate the spatiotemporal expression of
104 XAP5/XAP5L in various mouse tissues. We observed that XAP5 protein was widely
105 expressed in diverse tissues and present at all stages of postnatal testes maturation,

106 whereas XAP5L protein was mainly present in the testes and its level increased
107 dramatically from postnatal day 21 (P21) and continued into adulthood (Figures 1A, B).
108 Next, we identified the specific testicular cell types expressing XAP5/XAP5L using
109 published single-cell RNA-seq data(Jung et al., 2019). XAP5 mRNA was found
110 predominantly expressed in spermatogonia, while XAP5L mRNA was observed in
111 pachytene spermatocytes, and remained until elongating spermatids (Figure 1C).
112 Consistent with the mRNA localization patterns, immunofluorescence staining showed
113 that XAP5 protein was mainly detected in the nuclei of spermatogonia, whereas XAP5L
114 protein was present in the nuclei of pachytene spermatocytes and spermatids within the
115 seminiferous tubules, and neither of XAP5 or XAP5L was detected in mature sperm
116 (Figure 1D and Figure S1).

117 To investigate the physiological function of the uncharacterized XAP5/XAP5L protein,
118 we attempted to generate global KO mice using the CRISPR-Cas9 system. We
119 successfully established a *XAP5L* KO mouse line (Figures S2A-C) and found that while
120 all *XAP5L* KO mice survived to adulthood and appeared indistinguishable from the
121 wildtype (WT) mice, *XAP5L* KO males were sterile (Figures 1E, F). Notably, generating
122 mosaic F0 founders with *XAP5* mutant allele proved challenging, and no F1 generation
123 inherited the mutant alleles from the few F0 founders in over a year of breeding
124 experiments, underscoring the critical roles of XAP5 in mouse development.
125 Subsequently, we generated floxed-*XAP5* mice and crossed them with *Stra8-GFPCre*
126 knockin mice(Lin et al., 2017) to produce *XAP5* germline-specific KO mice (*XAP5* cKO)

127 (Figures S2D-F). Similar in appearance to controls (*XAP5*$^{fl/Y}$), all *XAP5* cKO males were
128 also found to be sterile (Figures 1G, H). Collectively, these results suggest that
129 XAP5/XAP5L play essential roles in spermatogenesis.

130 **XAP5 and XAP5L function at different stages of spermatogenesis**

131 To uncover the cause of male infertility, we conducted gross and histological analyses of
132 the testes from WT and *XAP5L* KO mice. There were no differences in the gross
133 appearance of testis or in the weight of mouse body and testis between WT and *XAP5L*
134 KO mice (Figure 2A), but the number of sperm collected from cauda epididymis of
135 *XAP5L* KO mice was significantly lower than that from WT mice (Figure 2B), and sperm
136 motility was significantly reduced in KO mice (Figure 2C and Videos S1, 2).
137 Histological analysis did not reveal any severe abnormity in the seminiferous epithelial
138 cycle of XAP5L KO testes (Figure 2D). Further examination of the morphology and
139 structure of cauda epididymal sperm in *XAP5L* KO mice revealed significantly higher
140 rates of abnormal flagella (Figures 2E-G), indicating that XAP5L is crucial for flagellar
141 assembly during spermiogenesis.

142 We also investigated the spermatogenic defects in the seminiferous tubules and
143 epididymis of *XAP5* cKO male mice. Notably, the testes of *XAP5* cKO males were
144 significantly smaller compared to WT controls at P16 and older (Figure 3A). Many
145 seminiferous tubules in P16 and older *XAP5* cKO males were vacuolated due to the
146 absence of spermatocytes and spermatids, as indicated by the lack of XY body formation
147 and the absence of PNA signal, a marker of spermatids and sperm, in *XAP5* cKO germ

148 cells (Figures 3B-D). As a consequence, no sperm were observed in the adult cauda
149 epididymides of *XAP5* cKO mice (Figure 3E). Taken together, these data indicate that
150 germ cell development in *XAP5* cKO males was arrested in meiotic prophase, and XAP5
151 is indispensable for meiotic progression during spermatogenesis.

152 **XAP5 and XAP5L function as antagonistic regulators of ciliary transcriptional**
153 **regulatory networks via regulating transcription factors**

154 To gain insight into the regulatory mechanisms of XAP5L during sperm flagellar
155 assembly, we employed RNA-seq analysis to examine mature sperm collected from the
156 cauda epididymis of WT and *XAP5L* KO adult mice. Differential expression analysis
157 identified 2093 upregulated and 267 downregulated genes in *XAP5L* KO sperm (Figure
158 S3A). Gene ontology analysis revealed that the upregulated genes were associated with
159 cilia assembly or function (Figure 4A and Figures S3B, C). When crossed with the
160 previously compiled ciliogenesis-related gene list(Nemajerova et al., 2016), the
161 upregulated genes were observed encompassing diverse structural and functional
162 components of the ciliogenic program (Table S1 and Figure S3D). Notably, several key
163 transcription factor (TF) regulators of ciliogenesis were among the upregulated genes,
164 including FOXJ1 and RFX families (Figures 4B, C and Figure S3E). Moreover, several
165 key regulators of spermatogenesis, particularly spermiogenesis, were identified, including
166 RFX2(Kistler et al., 2015; Wu et al., 2016), SOX families(Schartl et al., 2018; D. Zhang
167 et al., 2018), TAF7L(Zhou et al., 2013) and TBPL1(Martianov et al., 2001) (Figure 4B
168 and Figure S3E). Many core ciliary genes were also upregulated, such as

169 *CFAP206*(Beckers et al., 2020) and *IFT81*(Qu et al., 2020) which are critical for male
170 fertility (Figure S3E), consistent with the tight coregulation between spermiogenesis and
171 cilia-related genes during spermatogenesis. These findings suggest that the genes
172 identified in our study provide an excellent resource for candidates with novel ciliary or
173 spermatogenesis-related functions, and the newly identified testes-specific protein
174 TULP2(Oyama et al., 2022; Zheng et al., 2021) was selected for validation. We observed
175 that *TULP2* KO male mice were sterile due to malformation of sperm flagella (Figure
176 S4). Overall, our results clearly indicate that XAP5L acts as a central transcriptional
177 repressor of ciliogenesis during mouse spermatogenesis.

178 Furthermore, we performed RNA-seq analysis using P16 testes samples from WT and
179 *XAP5* cKO mice to explore the underlying mechanism of XAP5-mediated germ cell loss.
180 Differential expression analysis identified 554 upregulated and 1587 downregulated
181 genes in *XAP5* cKO sperm (Figure S5A). We observed that the downregulated genes in
182 *XAP5* cKO males were involved in cilium assembly or functions (Figure 4D and Figures
183 S5B-D). Strikingly, many of these downregulated genes were upregulated in *XAP5L* KO
184 sperm, including the key ciliogenesis regulators FOXJ1 and RFX families (Figures 4E, F,
185 Figure S5E and Table S1). In addition, meiosis initiation marker STRA8(Anderson et al.,
186 2008; Ferder et al., 2019), meiosis-specific genes SPO11(Romanienko & Camerini-
187 Otero, 2000) and DMC1(Bishop, Park, Xu, & Kleckner, 1992), key transcription
188 regulators of spermiogenesis RFX2(Kistler et al., 2015; Wu et al., 2016), SOX30(D.
189 Zhang et al., 2018) and CREM(Blendy, Kaestner, Weinbauer, Nieschlag, & Schutz, 1996;

190 Nantel et al., 1996) were also downregulated in *XAP5* cKO mice (Figures 4E and S5F),
191 consistent with the aforementioned result that loss of XAP5 induced spermatogenesis
192 arrest in meiotic stage.

193 To identify direct targets of XAP5/XAP5L, we conducted CUT&Tag analyses on P16
194 mouse testicular germ cells for XAP5, and on P56 mouse testicular germ cells for
195 XAP5L. Our results revealed 23143 peaks enriched for XAP5, compared to only 2290
196 peaks enriched for XAP5L (Table S1), and the limited number of enriched peaks for
197 XAP5L suggests that the antibody used for XAP5L in the CUT&Tag experiment might
198 have suboptimal performance. A substantial proportion of these peaks were located
199 within promoter regions (Figures S6A, B), indicating that XAP5/XAP5L primarily
200 function to regulate the expression of protein-coding genes. De novo motif analyses
201 showed that the binding motifs for XAP5 and XAP5L shared a conserved sequence
202 (CCCCGCCC/GGGCGGGG) (Figure S6C), suggesting that XAP5 may regulate a subset
203 of the same downstream genes as XAP5L.

204 To further elucidate the target genes of XAP5 and XAP5L, we integrated our
205 CUT&Tag data with RNA-seq datasets (Table S1). This analysis revealed that among the
206 genes downregulated in *XAP5* cKO germ cells, 891 were bound by XAP5 (Figure S6D).
207 Similarly, 75 genes upregulated in *XAP5L* KO sperm were occupied by XAP5L (Figure
208 S6E). GO analysis indicated that these genes are associated with cilium assembly and
209 related functions (Figures S6D-G). Notably, both *FOXJ1* and *RFX2* are regulated and
210 occupied by XAP5, with the conserved sequence present within the XAP5-bound regions

211 (Figure 4G). Furthermore, real-time PCR validation of the CUT&Tag experiments
212 confirmed that *RFX2* is also occupied by XAP5L, despite the initial CUT&Tag data not
213 showing enriched peaks for the RFX2 gene (Figure 4G). Unfortunately, due to the
214 suboptimal performance of the XAP5L antibody, we did not detect the occupancy of
215 XAP5L on the FOXJ1 promoter. Nevertheless, these findings suggest that XAP5 and
216 XAP5L regulate ciliary gene expression primarily through direct binding to the conserved
217 motif present in these genes.

218 Considering the evolutionary conservation of XAP5/XAP5L protein across different
219 species and the expression patterns of XAP5, XAP5L, FOXJ1 and RFX factors during
220 spermatogenesis (Figures 1C and S7), these results suggest that XAP5 and XAP5L have
221 antagonistic effects, and they may function upstream of the transcription factor families,
222 including FOXJ1 and RFX factors, to coordinate the ciliogenesis during spermatogenesis
223 (Figure 4H).

224

225 **Discussion**

226 Cilia and flagella are ancient organelles present in the last eukaryotic common ancestor
227 (LECA)(Mitchell, 2017). Cilia assembly and maintenance are under strict transcriptional
228 regulation in both unicellular and multicellular organisms(Choksi et al., 2014; Collins et
229 al., 2021; Lewis & Stracker, 2021; Thomas et al., 2010). Despite cilia and flagella having
230 an ancient origin, the evolutionary history of ciliary gene regulation has remained an
231 unsolved problem. The main reason is that the master ciliary transcription factors found

232 in multicellular organisms, including FOXJ1 and RFXs, are absent from unicellular
233 organisms(Choksi et al., 2014; Collins et al., 2021; Lewis & Stracker, 2021; Thomas et
234 al., 2010). Previously, we showed that an ancient transcription factor, XAP5, was
235 required for flagella assembly in the unicellular green algae *Chlamydomonas*(Li et al.,
236 2018). XAP5 proteins are evolutionarily conserved across diverse organisms(Li et al.,
237 2018; Martin-Tryon & Harmer, 2008), which offers the possibility to investigate the
238 conservation of the role of XAP5 in multicellular organisms. In the present study, we
239 report that XAP5 positively regulates transcriptional network of ciliary genes by
240 activating the key regulators including FOXJ1 and RFXs during spermatogenesis.

241 Cilia are dynamic organelles, and the expression profile of ciliary genes is dynamic
242 during the cell cycle and under certain physiological conditions(Eggenschwiler &
243 Anderson, 2007; Kasahara & Inagaki, 2021; Santos & Reiter, 2008). Cells have
244 developed regulatory mechanisms to generate functional cilia in a temporal and spatial
245 manner(Choksi et al., 2014; Collins et al., 2021; Lewis & Stracker, 2021; Thomas et al.,
246 2010). However, how ciliary transcription factors determine temporal and spatial ciliary
247 transcriptional programs is poorly understood. Sperm flagellar assembly is likewise
248 tightly regulated during a highly complex temporal process named
249 spermatogenesis(Holstein, Schulze, & Davidoff, 2003; Thomas et al., 2010). Several key
250 transcriptional regulators of spermatogenesis, such as FOXJ1 and RFX2, have been
251 identified(Chen, Knowles, Hebert, & Hackett, 1998; Kistler et al., 2015; Wu et al., 2016).
252 The flagellar formation of FOXJ1-null sperm is severely impaired, and the FOXJ1 target

253 genes are required for sperm motility(Beckers et al., 2020; Chen et al., 1998; Weidemann
254 et al., 2016). *RFX2* KO mice are completely sterile and RFX2 regulates the expression of
255 ciliary genes during spermiogenesis(Kistler et al., 2015; Wu et al., 2016). Ciliary
256 transcription factors (FOXJ1 and RFX2) are dynamically regulated during
257 spermatogenesis(Jung et al., 2019). Intriguingly, our results show that XAP5 and XAP5L
258 are two conserved pairs of antagonistic transcription factors that regulate these key
259 transcriptional regulators required for spermatogenesis.

260 By using Western blot analysis, we found that XAP5 was ubiquitously expressed in all
261 tissues examined, whereas XAP5L expression was restricted to the testes (Figure 1A).
262 Interestingly, previous research found that XAP5L was widely expressed in normal tissue
263 via using TCGA expression data(Thompson et al., 2021). Moreover, loss of
264 XAP5/XAP5L perturbs transcriptional programs in cancer cells. At present, as shown by
265 the recent data, we cannot rule out the possibility that XAP5L is dynamically expressed
266 in other tissues during development. Although XAP5 and XAP5L are highly expressed in
267 testes and critical for spermatogenesis, they are not present in mature sperm (Figure S1).
268 Thus, XAP5/XAP5L are not needed for sperm maintenance. Given the dynamic
269 expression of XAP5/XAP5L during spermatogenesis, it will be interesting to identify the
270 key signaling factors that regulate the timely and spatial expression of XAP5 and
271 XAP5L.

272 A role for XAP5 in human brain development is suggested by the association of X-
273 linked intellectual disability (XLID) with rare *XAP5* missense variants(Lee et al., 2020).

274 However, how defects in XAP5 lead to XLID syndrome is unknown. Although there is as
275 yet no evidence that XAP5 regulates ciliogenesis in any system besides *Chlamydomonas*
276 and mice, the function in cilia could help clarify the unexplained role of *XAP5* mutations
277 in causing XLID. The possibility that XAP5 could be a ciliary transcription factor in
278 humans would add XLID to the growing list of the second-order ciliopathies.
279
280

281 ## Materials and Methods

282 **Mice**

283 C57BL/6J strains (from Vital River Laboratories, Beijing, China) and *Stra8-GFPCre*
284 knockin mice (from Cyagen Biosciences) were used. Floxed-*XAP5* mice, *XAP5L* and
285 *TULP2* knockout mice were generated on the C57BL/6J background using the
286 CRISPR/Cas9 system. The sgRNA sequences used to target *XAP5*, *XAP5L* and *TULP2*
287 were as follows: *XAP5L*, sgRNA1-GGC TAC CAG AAA CAG GGA CT, sgRNA2-GGG
288 AGT AAG GTC CCC AAA CT; *XAP5*, sgRNA3-CTA CAG GGC ACT TAT TAA TA,
289 sgRNA4-ATA GTA ATT CCC CCG TGC TT; *TULP2*, sgRNA5-TGA CTA ATT AGG
290 CCC GAG AG, sgRNA6-GGT TCT TAG AGA GTC AAC GT. Experimental protocols
291 were approved by the ethics committees of Jianghan University. Mice were maintained in
292 a pathogen-free environment with a room temperature of 23 ± 2 °C under a humidity
293 level of 30-70%. The light was maintained on a 12-hour day/night cycle.
294

Genome PCR

Mouse genomic DNA was isolated from the tail tip using One Step Mouse Genotyping Kit (Vazyme, PD101), and subjected to PCR with 2 × Taq Plus Master Mix (Vazyme, P212) following the manufacturer's instructions. The PCR products were separated by 2% agarose gel electrophoresis. The primers used are listed in Table S2.

RNA isolation and real-time PCR

Total RNA was isolated using the TRIzol reagent (Invitrogen, 15596018) and then converted to cDNA with HiScript II 1st Strand cDNA Synthesis Kit (Vazyme, R212) following the manufacturer's instructions. Real-time PCR was conducted using ChamQ SYBR qPCR Master Mix (Vazyme, Q311) on an ABI StepOnePlus real-time PCR system (Applied Biosystems). Expression values were normalized using the ΔΔCt method with *Gapdh* as the internal control. The primer sequences are indicated in Table S2.

Western blot analysis

Cell lysates from mouse tissues were prepared in RIPA buffer (Beyotime, P0013B) containing Protease Inhibitor Cocktail (Roche, 11873580001) and 1mM PMSF. Subcellular lysates of testicular nuclear and cytoplasmic fractions were prepared using Nuclear and Cytoplasmic Protein Extraction Kit (Beyotime, P0027) following the manufacturer's instructions. The protein lysates were subjected to standard

immunoblotting analysis. Antibodies used were as follows: anti-β-actin (ABclonal, AC026), anti-XAP5 (Prospertech, HU-412003), anti-XAP5 (Sigma, HPA003585), anti-XAP5L (Prospertech, Hu-412001), anti-LMNB (Proteintech, 66095-1-Ig), anti-GAPDH (ABclonal, AC002), anti-FOXJ1 (D360355, Sangon Biotech), anti-RFX2 (K110716P, Solarbio) and anti-TULP2 (Prospertech, Hu-412002).

Immunofluorescence

Mouse testis were fixed in 4% paraformaldehyde in PBS at 4 °C overnight, dehydrated in gradient ethanol, embedded in paraffin, and sectioned into 5 μm slices. After deparaffinization and rehydration, testis sections were boiled in 1 mM EDTA, pH 8.0 for 15 min using a microwave oven for antigen retrieval, followed by cooling to room temperature. The primary antibodies, including anti-XAP5 (Prospertech, HU-412003, 1:250 dilution), anti-XAP5 (Sigma, HPA003585, 1:250 dilution), anti-XAP5L (Prospertech, Hu-412001, 1:250 dilution), anti-lectin PNA, Alexa Fluor 488 Conjugate (ThermoFisher, L21409, 1:250 dilution), and anti-TULP2 (Prospertech, Hu-412002, 1:250 dilution), were then incubated at 4 °C overnight. Subsequently, the sections were incubated with the secondary antibody donkey anti-rabbit Alexa Fluor Plus 488 (Invitrogen, A32790, 1:500 dilution) for 1 hour and DAPI for 5 minutes at room temperature. Images were collected using a Zeiss Axio Vert A1 microscope.

Histological analysis

Testes and epididymides were fixed in Bouin's solution (sigma, HT10132) overnight at 4 °C, embedded in paraffin and sectioned into 5 μm slices. The sections were then subjected to H&E staining using standard procedures and observed under a Zeiss Axio Vert A1 microscope.

Assessment of sperm counts, motility and morphology

Cauda epididymides were collected from male mice and dissected in 37°C pre-warmed human tubal fluid (HTF) culture medium (EasyCheck, M1130), followed by incubation at 37°C for 15 min to release the sperm. To quantify sperm abundance, the sperm suspension was fixed in 1% paraformaldehyde for 30 min. Sperm were then counted under a Zeiss ×10 bright-field microscope. To assess sperm motility, the sperm suspension was observed and recorded under a Leica total internal reflection fluorescence microscope. Motility was defined as any movement of the sperm flagellum during a 10-second observation cycle. After immobilization with 1% paraformaldehyde, sperm morphology was observed by H&E staining using standard procedures. Images were captured using a Zeiss Axio Vert A1 microscope equipped with a ×100 oil immersion objective. Sperm without staining were also used to assess sperm morphology. For ultrastructural observation, sperm samples were fixed in 3% glutaraldehyde in 0.1M sodium phosphate buffer (pH7.4), and post-fixed with 1% (wt/vol) OsO_4. After dehydration, the samples were placed in propylene oxide and embedded in a mixture of Epon 812 and Araldite. Ultrathin sections obtained by a Leica EM UC7 ultramicrotome

were stained with uranyl acetate and lead citrate, then analyzed using a HT7700 TEM (Hitachi).

Fertility test

Each of the adult male mice was mated with two females for 2 months. All the mice used were aged 6-8 weeks. Vaginal plugs were checked every morning, and the number of newborn pups was counted.

Chromosome spreads and immunofluorescence

Testicular chromosome spreads were prepared and immunolabeled as described(Reinholdt, Ashley, Schimenti, & Shima, 2004). The primary antibodies used were as follows: anti-γ H2AX (Millipore, 05-636, 1:300 dilution), anti-SYCP3 (Proteintech, 23024-1-AP, 1:300 dilution). Secondary antibodies used were Alexa Dye (AlexaFluor Plus 488/594) conjugates (ThermoFisher) at 1:500 dilutions. Images were collected with a Zeiss Axio Vert A1 microscope.

RNA-seq analysis

The mature sperm samples from P56 mice and testis samples from P16 mice were washed three time in 1× PBS after harvest. Total RNA was extracted from the samples using the TRIzol reagent (Invitrogen) and purified with the NEBNext Poly(A) mRNA Magnetic Isolation Module (NEB, E7490). The quality of the RNA samples was

examined using the Agilent 2100 Bioanalyzer system (Agilent Technologies). Qualified RNA samples were subjected to sequencing library construction using the NEBNext Ultra II RNA Library Prep Kit for Illumina (NEB, E7775). Paired-end (2 × 150 bp) sequencing was carried out on the Illumina NovaSeq6000 platform. The sequencing reads were mapped to the Mus musculus reference genome (GRCm38/mm10) using HISAT2 v2.1.0(Kim, Langmead, & Salzberg, 2015), and StringTie v1.3.3b(Pertea et al., 2015) was applied to assemble the mapped reads. Fragments Per Kilobase of transcript per Million fragments mapped (FPKM) was used to measure the expression level of a gene. Differential expression analysis was processed by DESeq2 v1.12.4(Subramanian et al., 2005), and the significant differentially expressed genes were identified with a fold change >2. Gene Ontology analysis was performed using the DAVID database.

CUT&Tag analysis

The testicular germ cells were isolated using a two-step enzymatic digestion process as previously described (Liu et al., 2017). Briefly, after removing the tunica albuginea, the testes were incubated in 1 mg/mL type IV collagenase (Sigma, C5138) at 37℃ for 15 min with gentle shaking every 5 min. The resulting cell suspension was centrifuged at 1000 rpm for 3 min, and the pellet was further digested with 0.25% Trypsin-EDTA (Gibco, 25200072) at 37℃ for 10 min. The digestion was terminated by adding fetal bovine serum (FBS), and the cell suspension was centrifuged at 1000 rpm for 3 min. The

cell pellet was resuspended in DMEM medium containing 10% FBS and cultured at 37℃ in a 5% CO2 atmosphere for 3 h. Floating and weakly adherent cells were collected as germ cells. CUT&Tag and CUT&Tag real-time PCR were performed according to the manufacturer's protocol using the Hyperactive Universal CUT&Tag Assay Kit for Illumina Pro (Vazyme, TD904). Approximately 100,000 germ cells were used per sample. For real-time PCR, IgG sera were used as a negative control for the XAP5 CUT&Tag, while lysates from *XAP5L* KO testis were incubated with the XAP5L antibody as a negative control for the XAP5L CUT&Tag. DNA spike in was used as the internal control. The primer sequences are indicated in Table S2.

For analysis, quality control and read trimming were performed using FastQC (v0.11.9) with default parameters and Trimmomatic (v0.39) with the following parameters: ILLUMINACLIP:NexteraPE-PE.fa:2:30:10:8:true LEADING:3 TRAILING:3 SLIDINGWINDOW:4:15 MINLEN:8. Clean reads were aligned with bowtie2 (v2.4.4)(Langmead & Salzberg, 2012) against the Mus musculus (mm39) genome with the parameters -X 1000 --very-sensitive. PCR duplicates were removed using picard's MarkDuplicates with default parameters. Peak calling was conducted using using MACS2 (v2.1.4) with the parameters -f BAMPE -B --SPMR --keep-dup all. Peaks were annotated to the nearest feature using ChIPseeker (v1.32.0)(G. Yu, Wang, & He, 2015). Motif finding and annotation were performed using Homer *findMotifsGenome.pl* and *annotatePeaks.pl* functions, respectively(Heinz et al., 2010). Track screen shots were produced in IGV (version 2.18.1)(Robinson, Thorvaldsdottir, Turner, & Mesirov, 2023).

Statistical analysis

Statistical analyses were conducted using GraphPad Prism 8.0.2 software. All data were presented as mean ± SEM. Values of $P < 0.05$ were considered statistically significant. Statistical significance between two groups was calculated using an unpaired, parametric, two-sided student's t test.

Materials and Data availability

The RNA-seq and CUT&Tag data generated in this study have been deposited in the Gene Expression Omnibus (GEO) database and are publicly available under accession numbers GSE236388 for RNA-seq and GSE279586 for CUT&Tag, respectively.

The authors declare that all the materials and the data supporting the findings of this study are available within the article and its supplementary materials or from the corresponding author upon reasonable request.

Acknowledgements

This work was supported by the National Key R&D Program of China (grant number: 2020YFA0907400), the National Natural Science Foundation of China (grant number: 32170702 and 82000828) and the Major Special Funding Program for First-class Discipline Construction of Jianghan University (grant number: 2023XKZ021). We thank Yuan He (Research Center for Medicine and Structural Biology, Wuhan University,

China) for the assistance during the experimental design of the transmission electron microscope analysis.

Author Contributions

W.W., J.X., X.Z. and Z.H. designed research; W.W., J.X., X.Z., H.L., X.L., H.J., C.X. and X.Z. performed research; W.W. and Z.H. contributed new reagents/analytic tools; W.W., J.X., X.Z. and Z.H. analyzed data; and W.W. and Z.H. wrote the paper.

Competing interests

The authors declare no competing interests.

Additional files

Table S1

The lists of differential expression genes, ciliogenesis-related genes, and enriched peaks for XAP5/XAP5L.

Table S2

The lists of primers used in the Genome PCR and real-time PCR.

Video S1

Representative video of living sperm cells from WT mouse.

Video S2

Representative video of living sperm cells from *XAP5L* KO mouse.

References

Anderson, E. L., Baltus, A. E., Roepers-Gajadien, H. L., Hassold, T. J., de Rooij, D. G., van Pelt, A. M., & Page, D. C. (2008). Stra8 and its inducer, retinoic acid, regulate meiotic initiation in both spermatogenesis and oogenesis in mice. *Proc Natl Acad Sci U S A, 105*(39), 14976-14980. doi:10.1073/pnas.0807297105

Beckers, A., Adis, C., Schuster-Gossler, K., Tveriakhina, L., Ott, T., Fuhl, F., . . . Gossler, A. (2020). The FOXJ1 target Cfap206 is required for sperm motility, mucociliary clearance of the airways and brain development. *Development*. doi:10.1242/dev.188052

Bishop, D. K., Park, D., Xu, L., & Kleckner, N. (1992). DMC1: a meiosis-specific yeast homolog of E. coli recA required for recombination, synaptonemal complex formation, and cell cycle progression. *Cell, 69*(3), 439-456. doi:10.1016/0092-8674(92)90446-j

Blendy, J. A., Kaestner, K. H., Weinbauer, G. F., Nieschlag, E., & Schutz, G. (1996). Severe impairment of spermatogenesis in mice lacking the CREM gene. *Nature, 380*(6570), 162-165. doi:10.1038/380162a0

Chen, J., Knowles, H. J., Hebert, J. L., & Hackett, B. P. (1998). Mutation of the mouse hepatocyte nuclear factor/forkhead homologue 4 gene results in an absence of cilia and random left-right asymmetry. *J Clin Invest, 102*(6), 1077-1082. doi:10.1172/JCI4786

Choksi, S. P., Lauter, G., Swoboda, P., & Roy, S. (2014). Switching on cilia: transcriptional networks regulating ciliogenesis. *Development, 141*(7), 1427-1441. doi:10.1242/dev.074666

Chu, J. S., Baillie, D. L., & Chen, N. (2010). Convergent evolution of RFX transcription factors and ciliary genes predated the origin of metazoans. *BMC Evol Biol, 10*, 130. doi:10.1186/1471-2148-10-130

Collins, C., Ventrella, R., & Mitchell, B. J. (2021). Building a ciliated epithelium: Transcriptional regulation and radial intercalation of multiciliated cells. *Curr Top Dev Biol, 145*, 3-39. doi:10.1016/bs.ctdb.2020.08.001

Derderian, C., Canales, G. I., & Reiter, J. F. (2023). Seriously cilia: A tiny organelle illuminates evolution, disease, and intercellular communication. *Dev Cell, 58*(15), 1333-1349. doi:10.1016/j.devcel.2023.06.013

Eggenschwiler, J. T., & Anderson, K. V. (2007). Cilia and developmental signaling. *Annu Rev Cell Dev Biol, 23*, 345-373. doi:10.1146/annurev.cellbio.23.090506.123249

Ferder, I. C., Fung, L., Ohguchi, Y., Zhang, X., Lassen, K. G., Capen, D., . . . Wang, N. (2019). Meiotic gatekeeper STRA8 suppresses autophagy by repressing Nr1d1 expression during spermatogenesis in mice. *PLoS Genet, 15*(5), e1008084. doi:10.1371/journal.pgen.1008084

Goetz, S. C., & Anderson, K. V. (2010). The primary cilium: a signalling centre during vertebrate development. *Nat Rev Genet, 11*(5), 331-344. doi:10.1038/nrg2774

Heinz, S., Benner, C., Spann, N., Bertolino, E., Lin, Y. C., Laslo, P., . . . Glass, C. K. (2010). Simple combinations of lineage-determining transcription factors prime cis-regulatory elements required for macrophage and B cell identities. *Mol Cell, 38*(4), 576-589. doi:10.1016/j.molcel.2010.05.004

Holstein, A.-F., Schulze, W., & Davidoff, M. (2003). Understanding spermatogenesis is a prerequisite for

treatment. *Reproductive Biology and Endocrinology, 1*(1). doi:10.1186/1477-7827-1-107

Ishikawa, H., & Marshall, W. F. (2011). Ciliogenesis: building the cell's antenna. *Nat Rev Mol Cell Biol, 12*(4), 222-234. doi:10.1038/nrm3085

Jung, M., Wells, D., Rusch, J., Ahmad, S., Marchini, J., Myers, S. R., & Conrad, D. F. (2019). Unified single-cell analysis of testis gene regulation and pathology in five mouse strains. *Elife, 8*. doi:10.7554/eLife.43966

Kasahara, K., & Inagaki, M. (2021). Primary ciliary signaling: links with the cell cycle. *Trends Cell Biol, 31*(12), 954-964. doi:10.1016/j.tcb.2021.07.009

Kim, D., Langmead, B., & Salzberg, S. L. (2015). HISAT: a fast spliced aligner with low memory requirements. *Nat Methods, 12*(4), 357-360. doi:10.1038/nmeth.3317

Kistler, W. S., Baas, D., Lemeille, S., Paschaki, M., Seguin-Estevez, Q., Barras, E., . . . Reith, W. (2015). RFX2 Is a Major Transcriptional Regulator of Spermiogenesis. *PLoS Genet, 11*(7), e1005368. doi:10.1371/journal.pgen.1005368

Langmead, B., & Salzberg, S. L. (2012). Fast gapped-read alignment with Bowtie 2. *Nat Methods, 9*(4), 357-359. doi:10.1038/nmeth.1923

Lee, Y.-R., Khan, K., Armfield-Uhas, K., Srikanth, S., Thompson, N. A., Pardo, M., . . . Schwartz, C. E. (2020). Mutations in FAM50A suggest that Armfield XLID syndrome is a spliceosomopathy. *Nature Communications, 11*(1). doi:10.1038/s41467-020-17452-6

Lewis, M., & Stracker, T. H. (2021). Transcriptional regulation of multiciliated cell differentiation. *Semin Cell Dev Biol, 110*, 51-60. doi:10.1016/j.semcdb.2020.04.007

Li, L., Tian, G., Peng, H., Meng, D., Wang, L., Hu, X., . . . Hu, Z. (2018). New class of transcription factors controls flagellar assembly by recruiting RNA polymerase II in Chlamydomonas. *Proc Natl Acad Sci U S A, 115*(17), 4435-4440. doi:10.1073/pnas.1719206115

Lin, Z., Hsu, P. J., Xing, X., Fang, J., Lu, Z., Zou, Q., . . . Tong, M. H. (2017). Mettl3-/Mettl14-mediated mRNA N(6)-methyladenosine modulates murine spermatogenesis. *Cell Res, 27*(10), 1216-1230. doi:10.1038/cr.2017.117

Liu, W., Wang, F., Xu, Q., Shi, J., Zhang, X., Lu, X., . . . Li, L. (2017). BCAS2 is involved in alternative mRNA splicing in spermatogonia and the transition to meiosis. *Nat Commun, 8*, 14182. doi:10.1038/ncomms14182

Lovera, M., & Lüders, J. (2021). The ciliary impact of nonciliary gene mutations. *Trends Cell Biol, 31*(11), 876-887. doi:10.1016/j.tcb.2021.06.001

Martianov, I., Fimia, G. M., Dierich, A., Parvinen, M., Sassone-Corsi, P., & Davidson, I. (2001). Late arrest of spermiogenesis and germ cell apoptosis in mice lacking the TBP-like TLF/TRF2 gene. *Mol Cell, 7*(3), 509-515. doi:10.1016/s1097-2765(01)00198-8

Martin-Tryon, E. L., & Harmer, S. L. (2008). XAP5 CIRCADIAN TIMEKEEPER coordinates light signals for proper timing of photomorphogenesis and the circadian clock in Arabidopsis. *Plant Cell, 20*(5), 1244-1259. doi:10.1105/tpc.107.056655

Mazzarella, R., Pengue, G., Yoon, J., Jones, J., & Schlessinger, D. (1997). Differential expression of XAP5, a candidate disease gene. *Genomics, 45*(1), 216-219. doi:10.1006/geno.1997.4912

Mitchell, D. R. (2017). Evolution of Cilia. *Cold Spring Harb Perspect Biol, 9*(1). doi:10.1101/cshperspect.a028290

542 Nachury, M. V., & Mick, D. U. (2019). Establishing and regulating the composition of cilia for signal
543 transduction. *Nat Rev Mol Cell Biol*. doi:10.1038/s41580-019-0116-4
544 Nantel, F., Monaco, L., Foulkes, N. S., Masquilier, D., LeMeur, M., Henriksen, K., . . . Sassone-Corsi, P.
545 (1996). Spermiogenesis deficiency and germ-cell apoptosis in CREM-mutant mice. *Nature,*
546 *380*(6570), 159-162. doi:10.1038/380159a0
547 Nemajerova, A., Kramer, D., Siller, S. S., Herr, C., Shomroni, O., Pena, T., . . . Lize, M. (2016). TAp73 is a
548 central transcriptional regulator of airway multiciliogenesis. *Genes Dev, 30*(11), 1300-1312.
549 doi:10.1101/gad.279836.116
550 Oyama, Y., Miyata, H., Shimada, K., Larasati, T., Fujihara, Y., & Ikawa, M. (2022). TULP2 deletion mice
551 exhibit abnormal outer dense fiber structure and male infertility. *Reprod Med Biol, 21*(1), e12467.
552 doi:10.1002/rmb2.12467
553 Pertea, M., Pertea, G. M., Antonescu, C. M., Chang, T.-C., Mendell, J. T., & Salzberg, S. L. (2015).
554 StringTie enables improved reconstruction of a transcriptome from RNA-seq reads. *Nature*
555 *Biotechnology, 33*(3), 290-295. doi:10.1038/nbt.3122
556 Piasecki, B. P., Burghoorn, J., & Swoboda, P. (2010). Regulatory Factor X (RFX)-mediated transcriptional
557 rewiring of ciliary genes in animals. *Proc Natl Acad Sci U S A, 107*(29), 12969-12974.
558 doi:10.1073/pnas.0914241107
559 Qu, W., Yuan, S., Quan, C., Huang, Q., Zhou, Q., Yap, Y., . . . Zhang, Z. (2020). The essential role of
560 intraflagellar transport protein IFT81 in male mice spermiogenesis and fertility. *Am J Physiol Cell*
561 *Physiol, 318*(6), C1092-C1106. doi:10.1152/ajpcell.00450.2019
562 Reinholdt, L., Ashley, T., Schimenti, J., & Shima, N. (2004). Forward genetic screens for meiotic and
563 mitotic recombination-defective mutants in mice. *Methods Mol Biol, 262*, 87-107. doi:10.1385/1-
564 59259-761-0:087
565 Reiter, J. F., & Leroux, M. R. (2017). Genes and molecular pathways underpinning ciliopathies. *Nat Rev*
566 *Mol Cell Biol, 18*(9), 533-547. doi:10.1038/nrm.2017.60
567 Robinson, J. T., Thorvaldsdottir, H., Turner, D., & Mesirov, J. P. (2023). igv.js: an embeddable JavaScript
568 implementation of the Integrative Genomics Viewer (IGV). *Bioinformatics, 39*(1).
569 doi:10.1093/bioinformatics/btac830
570 Romanienko, P. J., & Camerini-Otero, R. D. (2000). The mouse Spo11 gene is required for meiotic
571 chromosome synapsis. *Mol Cell, 6*(5), 975-987. doi:10.1016/s1097-2765(00)00097-6
572 Santos, N., & Reiter, J. F. (2008). Building it up and taking it down: the regulation of vertebrate
573 ciliogenesis. *Dev Dyn, 237*(8), 1972-1981. doi:10.1002/dvdy.21540
574 Schartl, M., Schories, S., Wakamatsu, Y., Nagao, Y., Hashimoto, H., Bertin, C., . . . Herpin, A. (2018). Sox5
575 is involved in germ-cell regulation and sex determination in medaka following co-option of nested
576 transposable elements. *BMC Biol, 16*(1), 16. doi:10.1186/s12915-018-0485-8
577 Sedlacek, Z., Munstermann, E., Dhorne-Pollet, S., Otto, C., Bock, D., Schutz, G., & Poustka, A. (1999).
578 Human and mouse XAP-5 and XAP-5-like (X5L) genes: identification of an ancient functional
579 retroposon differentially expressed in testis. *Genomics, 61*(2), 125-132.
580 doi:10.1006/geno.1999.5931
581 Singla, V., & Reiter, J. F. (2006). The primary cilium as the cell's antenna: signaling at a sensory organelle.
582 *Science, 313*(5787), 629-633. doi:10.1126/science.1124534

583 Stubbs, J. L., Oishi, I., Izpisua Belmonte, J. C., & Kintner, C. (2008). The forkhead protein Foxj1 specifies
584 node-like cilia in Xenopus and zebrafish embryos. *Nat Genet, 40*(12), 1454-1460.
585 doi:10.1038/ng.267
586 Subramanian, A., Tamayo, P., Mootha, V. K., Mukherjee, S., Ebert, B. L., Gillette, M. A., . . . Mesirov, J. P.
587 (2005). Gene set enrichment analysis: A knowledge-based approach for interpreting genome-wide
588 expression profiles. *Proceedings of the National Academy of Sciences, 102*(43), 15545-15550.
589 doi:10.1073/pnas.0506580102
590 Swoboda, P., Adler, H. T., & Thomas, J. H. (2000). The RFX-type transcription factor DAF-19 regulates
591 sensory neuron cilium formation in C. elegans. *Mol Cell, 5*(3), 411-421. doi:10.1016/s1097-
592 2765(00)80436-0
593 Thomas, J., Morle, L., Soulavie, F., Laurencon, A., Sagnol, S., & Durand, B. (2010). Transcriptional control
594 of genes involved in ciliogenesis: a first step in making cilia. *Biol Cell, 102*(9), 499-513.
595 doi:10.1042/BC20100035
596 Thompson, N. A., Ranzani, M., van der Weyden, L., Iyer, V., Offord, V., Droop, A., . . . Adams, D. J.
597 (2021). Combinatorial CRISPR screen identifies fitness effects of gene paralogues. *Nature*
598 *Communications, 12*(1). doi:10.1038/s41467-021-21478-9
599 Vij, S., Rink, J. C., Ho, H. K., Babu, D., Eitel, M., Narasimhan, V., . . . Roy, S. (2012). Evolutionarily
600 ancient association of the FoxJ1 transcription factor with the motile ciliogenic program. *PLoS*
601 *Genet, 8*(11), e1003019. doi:10.1371/journal.pgen.1003019
602 Weidemann, M., Schuster-Gossler, K., Stauber, M., Wrede, C., Hegermann, J., Ott, T., . . . Gossler, A.
603 (2016). CFAP157 is a murine downstream effector of FOXJ1 that is specifically required for
604 flagellum morphogenesis and sperm motility. *Development, 143*(24), 4736-4748.
605 doi:10.1242/dev.139626
606 Wu, Y., Hu, X., Li, Z., Wang, M., Li, S., Wang, X., . . . Han, C. (2016). Transcription Factor RFX2 Is a Key
607 Regulator of Mouse Spermiogenesis. *Sci Rep, 6*, 20435. doi:10.1038/srep20435
608 Yu, G., Wang, L. G., & He, Q. Y. (2015). ChIPseeker: an R/Bioconductor package for ChIP peak
609 annotation, comparison and visualization. *Bioinformatics, 31*(14), 2382-2383.
610 doi:10.1093/bioinformatics/btv145
611 Yu, X., Ng, C. P., Habacher, H., & Roy, S. (2008). Foxj1 transcription factors are master regulators of the
612 motile ciliogenic program. *Nat Genet, 40*(12), 1445-1453. doi:10.1038/ng.263
613 Zhang, A., Skaar, D. A., Li, Y., Huang, D., Price, T. M., Murphy, S. K., & Jirtle, R. L. (2011). Novel
614 retrotransposed imprinted locus identified at human 6p25. *Nucleic Acids Res, 39*(13), 5388-5400.
615 doi:10.1093/nar/gkr108
616 Zhang, D., Xie, D., Lin, X., Ma, L., Chen, J., Zhang, D., . . . Han, C. (2018). The transcription factor
617 SOX30 is a key regulator of mouse spermiogenesis. *Development, 145*(11).
618 doi:10.1242/dev.164723
619 Zheng, M., Chen, X., Cui, Y., Li, W., Dai, H., Yue, Q., . . . Zhu, H. (2021). TULP2, a New RNA-Binding
620 Protein, Is Required for Mouse Spermatid Differentiation and Male Fertility. *Front Cell Dev Biol,*
621 *9*, 623738. doi:10.3389/fcell.2021.623738
622 Zhou, H., Grubisic, I., Zheng, K., He, Y., Wang, P. J., Kaplan, T., & Tjian, R. (2013). Taf7l cooperates with
623 Trf2 to regulate spermiogenesis. *Proc Natl Acad Sci U S A, 110*(42), 16886-16891.

doi:10.1073/pnas.1317034110

626 **Figures**

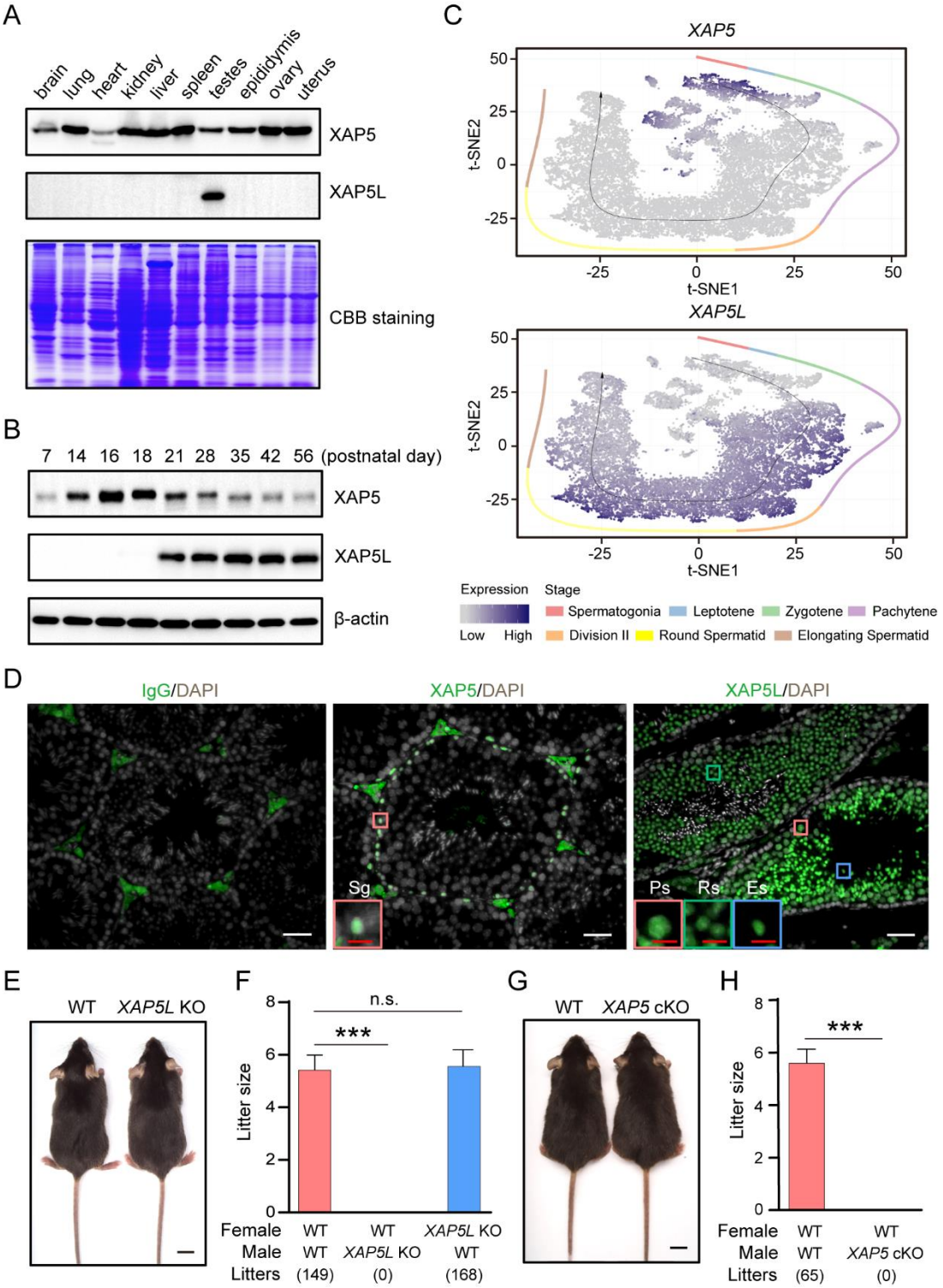

627

628 **Figure 1. Loss of XAP5 and XAP5L proteins results in male mice infertility.**

629 **(A)** Detection of XAP5/XAP5L protein in different tissues of adult mice by Western blot
630 analysis. **(B)** Expression of XAP5/XAP5L protein during postnatal testicular
631 development. β-actin was used as control. **(C)** t-SNE plots displaying *XAP5*/*XAP5L* gene
632 expression levels in individual cell types of mouse testis visualized using published
633 single-cell data(Jung et al., 2019). Black arrow represents the developmental pseudotime
634 corresponding to the developmental ordering of each cell progressing through
635 spermatogenesis. Dot color intensity represents the expression level. Cells from different
636 stages are color-coded. **(D)** Immunofluorescence staining of XAP5/XAP5L in adult WT
637 testis. Representative spermatogonium (Sg), round spermatid (Rs) and elongating
638 spermatid (Es) are indicated. Scale bars: 20 μm (white), 5 μm (red). **(E)** Similar
639 development between WT and *XAP5L* KO mice. Scale bar: 1 cm. **(F)** Average litter size
640 of pups obtained by fertility test. Each male was caged with two females for 2 months, 5
641 males were used for each genotype. ***$P < 0.001$, n.s. stands for not significant. **(G)**
642 Similar appearance of WT and *XAP5* cKO mice. Scale bar: 1 cm. **(H)** Average litter size
643 of pups obtained by fertility test. Each male was caged with two WT females for 2
644 months, 4 males were used for each genotype. ***$P < 0.001$. Error bars depict means ±
645 SEM. All *P*-values were calculated using an unpaired, two-tailed Student's t-test.

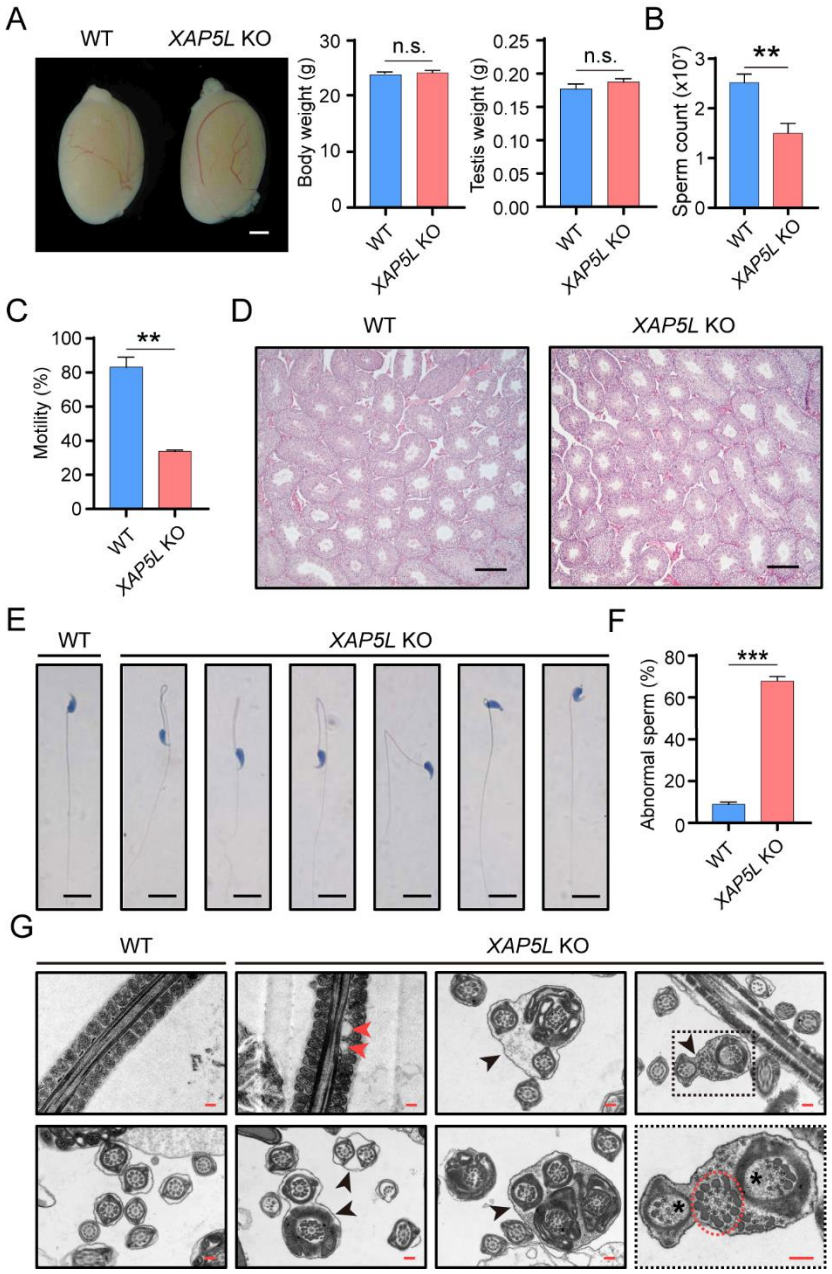

646

647 **Figure 2. XAP5L is required for normal sperm formation.**

648 **(A)** Similar gross testes morphology, body weight and testis weight between WT and

649 *XAP5L* KO mice. Scale bar: 1 mm. n = 6, n.s. stands for not significant. **(B)** Significantly

650 reduced caudal epididymal sperm counts in XAP5L KO mice compared with WT males.

651 n = 5, $^{**}P < 0.01$. **(C)** Significantly reduced sperm total motility of *XAP5L* KO mice. n =

652 3, **$P < 0.01$. **(D)** H&E staining showing similar histological structure of the testes from
653 WT and *XAP5L* KO mice. Scale bars: 100 μm. **(E)** H&E staining showing the
654 morphology of sperm in WT and *XAP5L* KO mice. Scale bars: 10 μm. **(F)** Significantly
655 increased abnormal sperm in *XAP5L* KO mice. n = 6, ***$P < 0.001$. **(G)** Electron
656 microscopic analysis displaying ultrastructural defects in *XAP5L* KO sperm flagella,
657 including cytoplasmic vacuoles enveloping mitochondrial sheath (as shown by red
658 arrowheads), a complete lack of mitochondrial sheath (as shown by red dotted circle),
659 two or more cross-sections of the same sperm flagellum enclosed within one cell
660 membrane (as shown by black arrowheads), partially formed outer dense fibers, and the
661 axonemal microtubules (as indicated by asterisks). Scale bars: 2 μm. Error bars depict
662 means ± SEM. All *P*-values were calculated using an unpaired, two-tailed Student's t-
663 test.

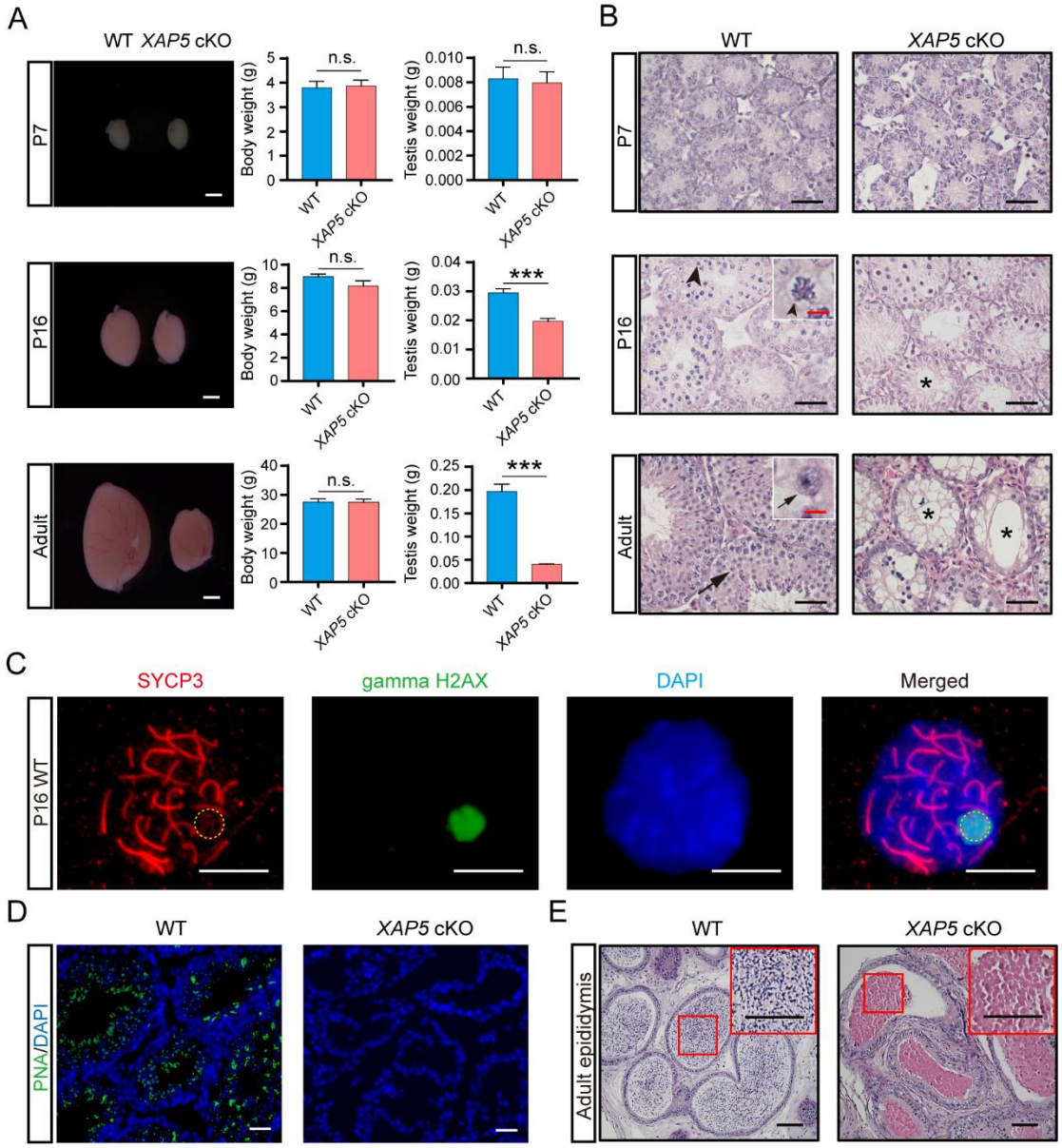

Figure 3. Ablation of XAP5 in germ cells results in arrested spermatogenesis and absence of sperm.

(A) Testes sizes, body weight and testis weight from WT and *XAP5* cKO mice at various ages were evaluated. Similar body weight was observed between WT and *XAP5* cKO mice. No significant difference in size and weight was detected between WT and *XAP5* cKO testes until P16. Scale bars: 1 mm. n = 5, ***$P < 0.001$, n.s. stands for not

671 significant. **(B)** Histology of testes from WT and *XAP5* cKO mice at various ages were
672 evaluated by H&E staining. No pachytene spermatocytes were found, and many
673 vacuolated tubules were observed in *XAP5* cKO testis since P16. Black arrowheads
674 indicate pachytene spermatocytes; black arrows indicate round spermatids. Vacuolated
675 seminiferous tubules are indicated by asterisks. Scale bars: 20 μm (black), 2.5 μm (red).
676 **(C)** Chromosome spreads staining showing pachytene spermatocytes from P16 WT male
677 mouse. Yellow dotted circle indicates the XY body. Scale bars: 10 μm. **(D)**
678 Immunofluorescence staining of PNA in adult testes indicating the absence of spermatids
679 in *XAP5* cKO mice. Scale bars: 20 μm. **(E)** H&E staining of adult epididymis displaying
680 absence of sperm in *XAP5* cKO mice. Scale bars: 50 μm. Error bars depict means ± SEM.
681 All *P*-values were calculated using an unpaired, two-tailed Student's t-test.

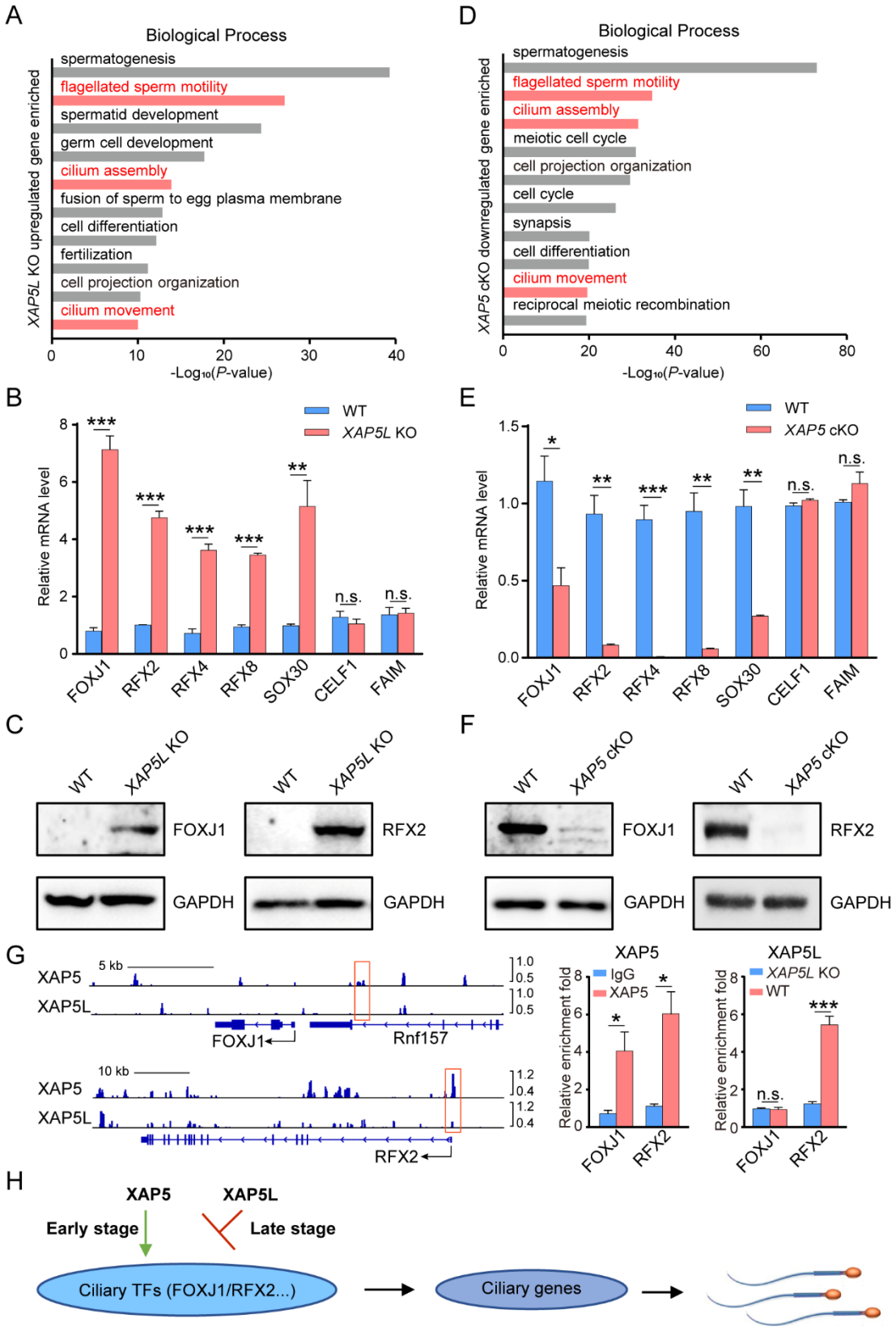

682

683 **Figure 4. Aberrant ciliogenic and spermatogenic gene expression in *XAP5L* KO and**

684 ***XAP5* cKO male germ cells.**

685 **(A)** Gene ontology analysis showing top ten biological process terms significantly
686 enriched among upregulated genes in *XAP5L* KO sperm. **(B)** Real-time PCR validation of
687 genes involved in ciliogenesis and spermatogenesis. n = 3, $^{**}P < 0.01$, $^{***}P < 0.001$, n.s.
688 stands for not significant. **(C)** Detection of FOXJ1 and RFX2 in mature sperm of WT and
689 *XAP5L* KO mice by Western blot analysis. GAPDH was used as a control. **(D)** Gene
690 ontology analysis showing top ten biological process terms significantly enriched among
691 downregulated genes in P16 *XAP5* cKO testes. **(E)** Real-time PCR validation of genes
692 involved in ciliogenesis and spermatogenesis. n = 3, $^{*}P < 0.05$, $^{**}P < 0.01$, $^{***}P < 0.001$,
693 n.s. stands for not significant. **(F)** Detection of FOXJ1 and RFX2 in P16 testes of WT and
694 *XAP5* cKO mice by Western blot analysis. GAPDH was used as a control. **(G)**
695 XAP5/XAP5L occupancies at *FOXJ1* and *RFX2* promoters assessed by CUT&Tag-seq
696 (left) and CUT&Tag real-time PCR (middle and right). Red boxes indicate the binding
697 regions of XAP5 and XAP5L. n = 3, $^{*}P < 0.05$, $^{***}P < 0.001$, n.s. stands for not
698 significant. **(H)** A model on the involvement of XAP5 and XAP5L in the regulation of
699 ciliogenesis during spermatogenesis. Error bars depict means ± SEM. All *P*-values were
700 calculated using an unpaired, two-tailed Student's t-test.

701

702

703

704

705 **Supplementary Figures**

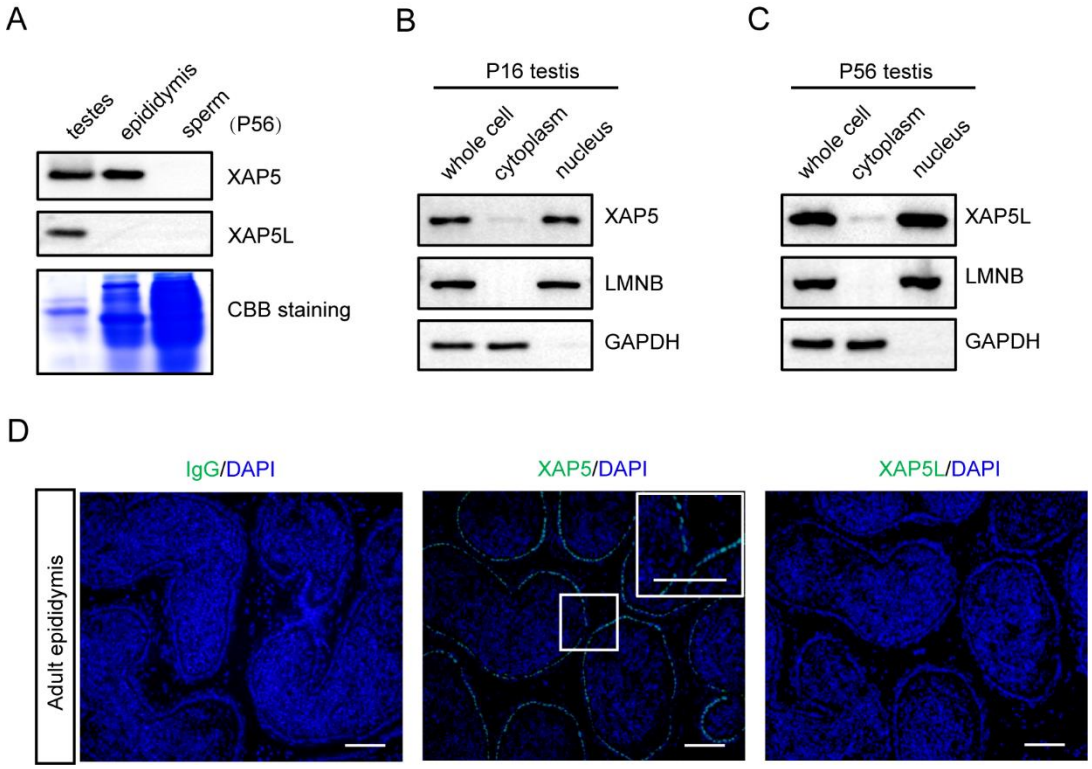

706

707 **Figure S1. Localization of XAP5/XAP5L in testicular cells.**

708 **(A)** Western blot analysis showing no localization of XAP5/XAP5L in mature sperm.
709 Western blot analysis showing the subcellular localization of endogenous XAP5 (**B**) and
710 XAP5L (**C**). LMNB used as a nuclear protein marker, GAPDH used as a cytoplasmic
711 protein marker. **(D)** Immunofluorescence staining of XAP5/XAP5L in adult epididymis.
712 Scale bars: 50 μm.

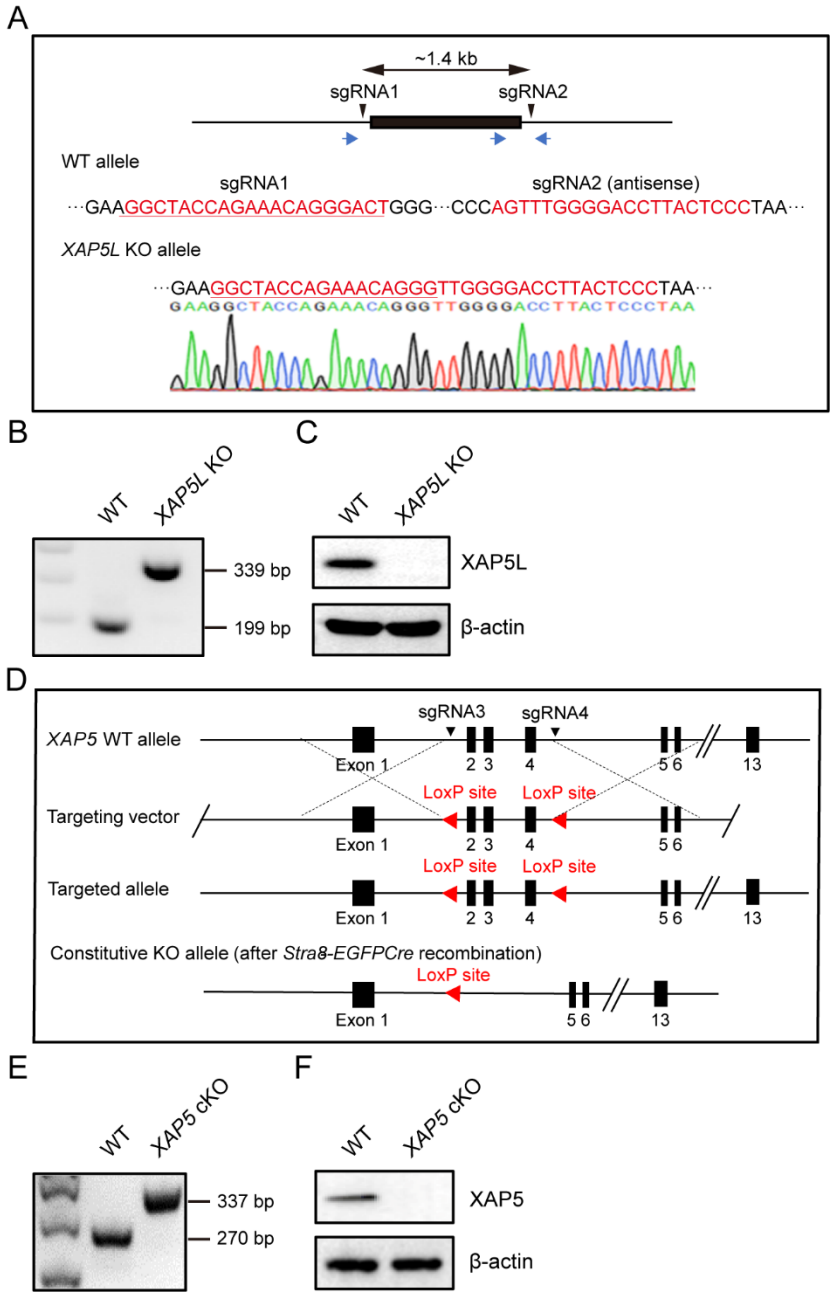

Figure S2. Generation of *XAP5L* KO and *XAP5* cKO mice.

(A) Schematic illustration of the targeting strategy for generating a *XAP5L* knockout mouse line using CRISPR-Cas9 system. Upper panel showing genomic structure of the *XAP5L* gene. The location of two sgRNAs (sgRNA1 and sgRNA2) used and three primers (blue arrows) for genome PCR are indicated. Lower panel displaying nucleotide

719 sequence of WT allele in the vicinity of two sgRNAs (red color) and the corresponding
720 sequence of the *XAP5L* homozygous mutant (KO) allele. The deletion of *XAP5L* gene
721 was verified by Sanger sequencing. **(B)** Genome PCR analysis in WT and *XAP5L* KO
722 mice. **(C)** Detection of XAP5L in adult testes extracts of WT and *XAP5L* KO mice by
723 Western blot analysis. β-actin was used as a control. **(D)** Schematic illustration of the
724 targeting strategy for generating *XAP5* cKO mice. The location of LoxP sites inserted and
725 the primers (blue arrow) used for genome PCR are indicated. **(E)** Genome PCR analysis
726 in WT and *XAP5* cKO mice. **(F)** Detection of XAP5 in testes extracts of WT and *XAP5*
727 cKO mice by Western blot analysis. β-actin was used as a control.

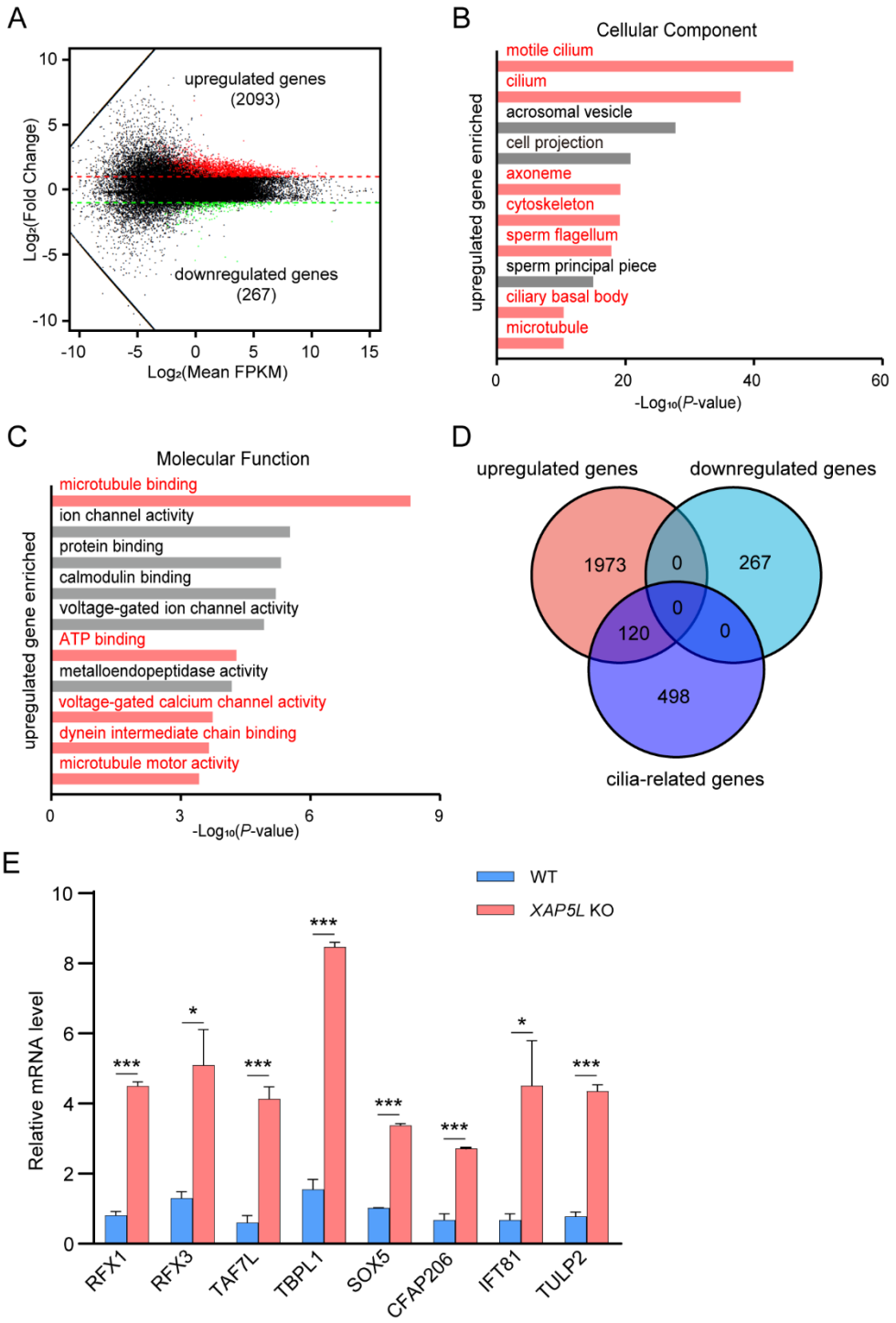

728

729 **Figure S3. XAP5L-mediated regulation of ciliary gene expression during mouse**

730 **spermatogenesis.**

731 **(A)** MA plot showing the numbers of differentially expressed genes in *XAP5L* KO sperm.

732 Gene ontology analysis showing top ten cellular component (**B**) and molecular function
733 (**C**) terms significantly enriched among upregulated genes in *XAP5L* KO sperm. **(D)** Venn
734 diagram representing total genes upregulated/downregulated by at least twofold in
735 *XAP5L* KO sperm and published cilia-related genes(Nemajerova et al., 2016). **(E)** Real-
736 time PCR validation of genes involved in ciliogenesis and spermatogenesis. n = 3, *$P <$
737 0.05, ***$P < 0.001$. Error bars depict means ± SEM. All P-values were calculated using
738 an unpaired, two-tailed Student's t-test.

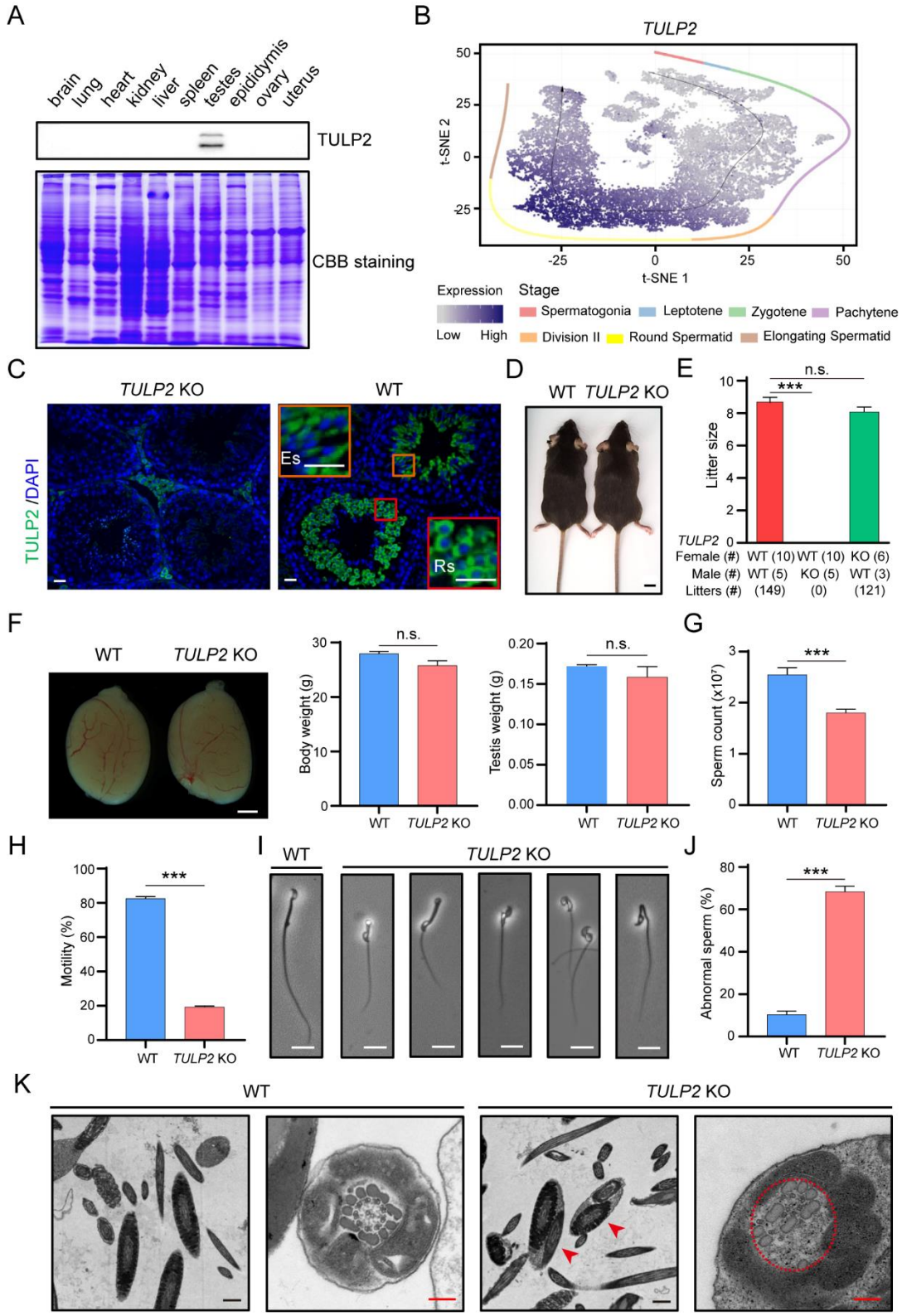

739

740 **Figure S4. *TULP2* KO male mice were infertile due to malformation of sperm.**

741 **(A)** Detection of TULP2 protein in different tissues of adult mice by Western blot

742 analysis. **(B)** t-SNE plot displaying *TULP2* gene expression pattern during
743 spermatogenesis visualized using published single-cell data(Jung et al., 2019). Black
744 arrow represents the developmental pseudotime corresponding to the developmental
745 ordering of each cell progressing through spermatogenesis. Dot color intensity represents
746 the expression level. Cells from different stages are color-coded. **(C)**
747 Immunofluorescence staining showing TULP2 expression in the cytoplasm of round
748 spermatids (Rs) and elongating spermatids (Es). Scale bars: 5 μm. **(D)** Similar
749 development of adult WT and *TULP2* KO mice. Scale bar: 1 cm. **(E)** Average litter size
750 of pups obtained by fertility test. Each male was caged with two females for 2 months.
751 ***$P < 0.001$, n.s. stands for not significant. **(F)** Similar gross testes morphology, body
752 weight and testis weight between WT and *TULP2* KO mice. Scale bar: 1 mm. n = 4, n.s.
753 stands for not significant. **(G)** Significantly reduced caudal epididymal sperm counts in
754 *TULP2* KO mice compared with WT males. n = 7, ***$P < 0.001$. **(H)** Significantly
755 reduced sperm total motility of *TULP2* KO mice. n = 3, ***$P < 0.001$. Significantly
756 increased abnormal sperm in *TULP2* KO mice (**I** and **J**). Scale bars: 10 μm. n = 3, ***$P <$
757 0.001. **(K)** Electron microscopic analysis displaying ultrastructural defects in *TULP2* KO
758 sperm flagella, including two cross-sections of the same sperm flagellum enclosed within
759 one cell membrane (as shown by red arrowheads), disorganized outer dense fibers and the
760 axonemal microtubules (as shown by red dotted circle). Scale bars: 8 μm (black), 2 μm
761 (red). Error bars depict means ± SEM. All *P*-values were calculated using an unpaired,
762 two-tailed Student's t-test.

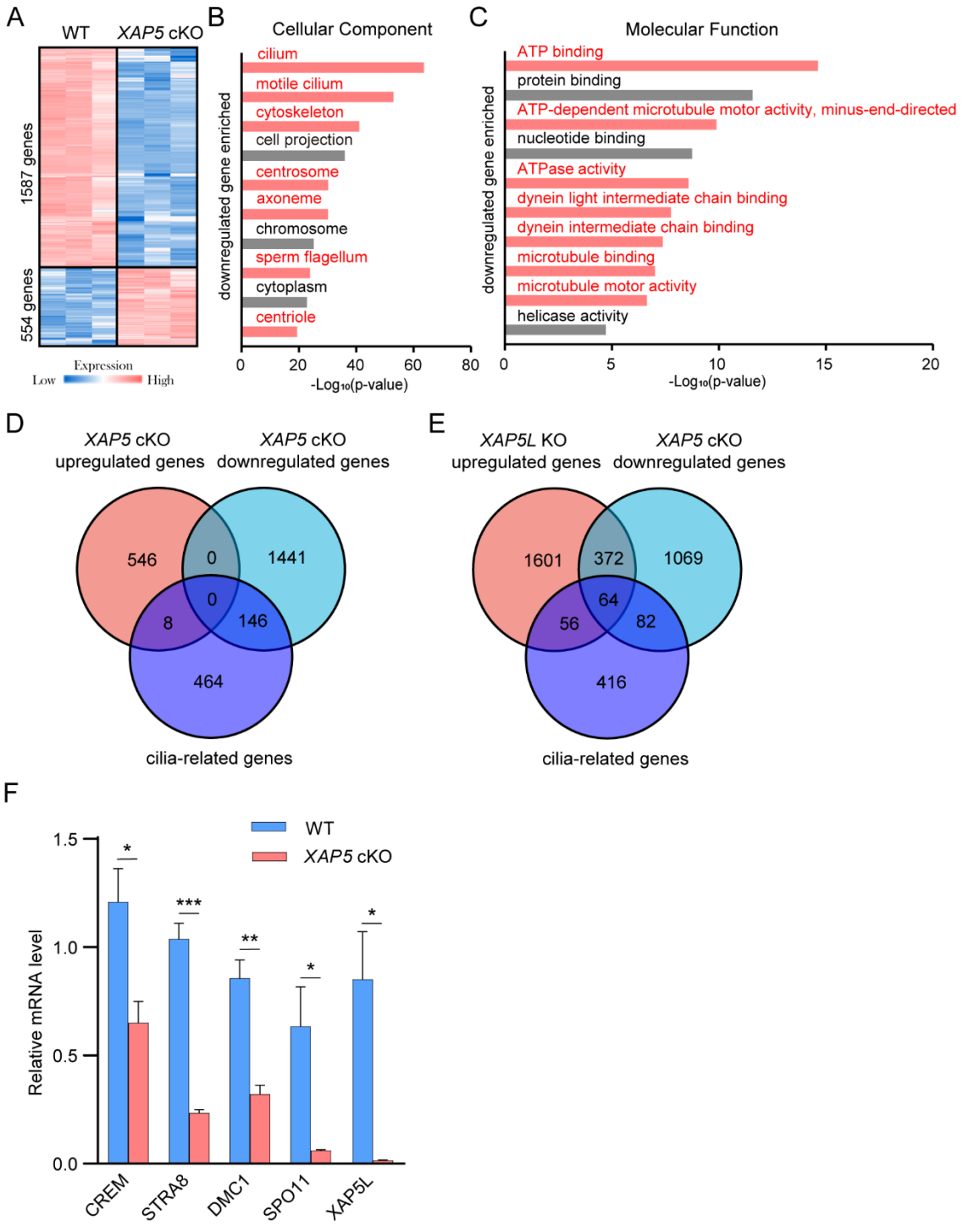

Figure S5. XAP5-mediated regulation of ciliary gene expression during mouse spermatogenesis.

(A) Heat map showing variably expressed genes in P16 *XAP5* cKO testes. Number of

767 related genes was indicated. Gene ontology analysis showing top ten cellular component
768 (**B**) and molecular function (**C**) terms significantly enriched among downregulated genes
769 in *XAP5* cKO testes. **(D)** Venn diagram representing total genes
770 upregulated/downregulated in *XAP5* cKO testes and published cilia-related
771 genes(Nemajerova et al., 2016). **(E)** Venn diagram representing total genes
772 downregulated in *XAP5* cKO testes, upregulated in *XAP5L* KO sperm by at least twofold
773 and published cilia-related genes(Nemajerova et al., 2016). **(F)** Real-time PCR validation
774 of genes involved in ciliogenesis and spermatogenesis. n = 3, **P* < 0.05, ***P* < 0.01, ****P*
775 < 0.001. Error bars depict means ± SEM. All *P*-values were calculated using an unpaired,
776 two-tailed Student's t-test.

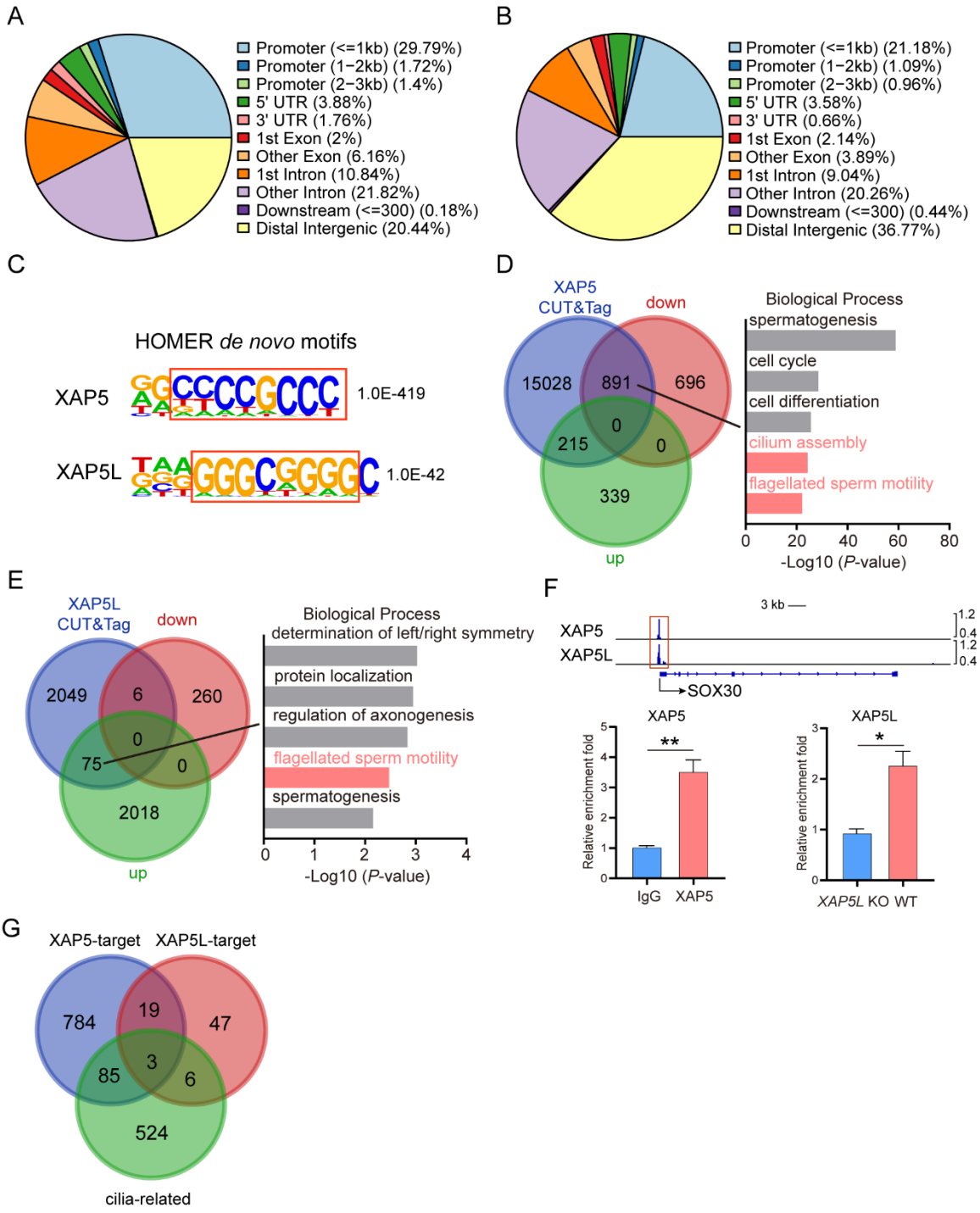

Figure S6. Identification of XAP5/XAP5L-occupancy sites

Location of XAP5 **(A)** and XAP5L **(B)**-occupancy peaks relative to the nearest annotated gene. **(C)** DNA sequence identified by Homer de novo motif analysis from

781 XAP5/XAP5L peaks. The P value of the motif comparison is indicated. Overlapped
782 sequences are shown in red boxes. (**D**) Left, overlapping genes identified by XAP5
783 CUT&Tag and RNA-seq analyses. Right, representative biological processes enriched
784 among the overlapping genes that are downregulated in *XAP5* cKO germ cells and bound
785 by XAP5 (as identified by CUT&Tag). (**E**) Left, overlapping genes identified by XAP5L
786 CUT&Tag and RNA-seq analyses. Right, representative biological processes enriched
787 among the overlapping genes that are upregulated in *XAP5* KO sperm and bound by
788 XAP5L (as identified by CUT&Tag). (**F**) XAP5/XAP5L occupancies at *SOX30* promoter
789 assessed by CUT&Tag-seq (top) and CUT&Tag real-time PCR (bottom). Red boxes
790 indicate the binding regions of XAP5/XAP5L. n = 3, $^{*}P < 0.05$, $^{**}P < 0.01$. (**G**)
791 Overlapping genes among XAP5/XAP5L target genes (the 891 genes in Figure S6D and
792 the 75 genes in Figure S6E) and published cilia-related genes(Nemajerova et al., 2016).
793 Error bars depict means ± SEM. All *P*-values were calculated using an unpaired, two-
794 tailed Student's t-test.

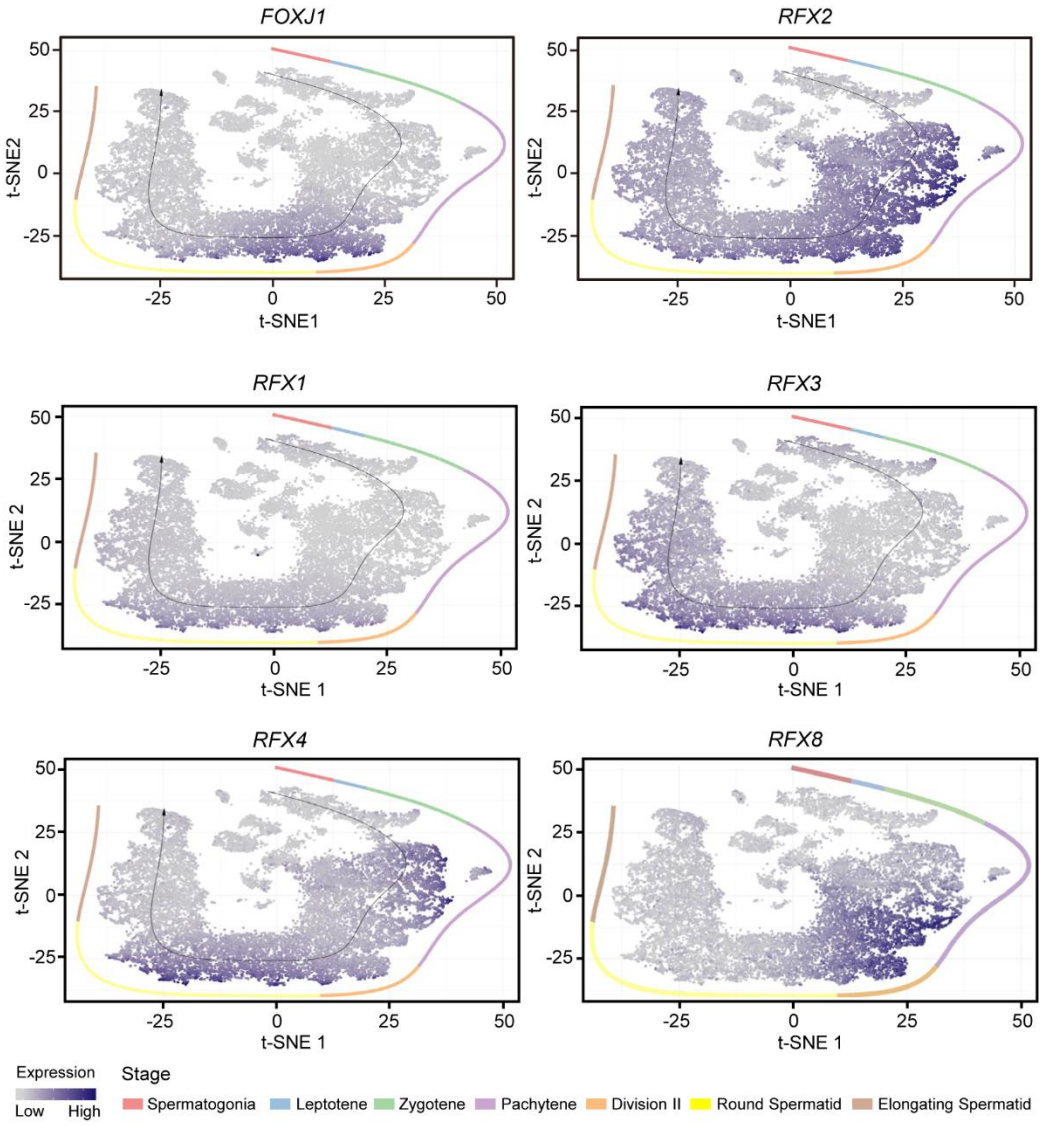

Figure S7. t-SNE plots displaying expression patterns of *FOXJ1* and *RFX* families in individual cell types of mouse testes.

The black arrow represents the developmental pseudotime corresponding to the developmental ordering of each cell progressing through spermatogenesis. Dot color intensity represents the relative expression level. Cells from different stages are color-coded. The gene expression was visualized using the published single-cell data(Jung et al., 2019).